Met. Mater. Int., Vol. 21, No. 5 (2015), pp. 805~814
doi: 10.1007/s12540-015-5094-2

Effect of Rolling Asymmetry on Selected Properties of Grade 2 Titanium Sheet

M. Wroński[1,3], K. Wierzbanowski[1,*], M. Wróbel[2], S. Wroński[1], and B. Bacroix[3]

[1]Faculty of Physics and Applied Computer Science, AGH University of Science and Technology, al. Mickiewicza 30, 30-059 Kraków, Poland
[2]Faculty of Metals Engineering and Industrial Computer Science, AGH University of Science and Technology, al. Mickiewicza 30, 30-059 Kraków, Poland
[3]LSPM-CNRS, Université Paris XIII, Sorbonne Paris Cité, 99, av. J.B. Clement, 93 430 Villetaneuse, France

(received date: 13 February 2015 / accepted date: 27 May 2015)

Asymmetric rolling can be used in order to modify material properties and to reduce forces and torques applied during deformation. This geometry of deformation is relatively easy to implement on existing industrial rolling mills and it can provide large volumes of a material. The study of microstructure, crystallographic texture and residual stress in asymmetrically rolled titanium (grade 2) is presented in this work. The above characteristics were examined using the EBSD technique and X-ray diffraction. The rolling asymmetry was realized using two identical rolls, driven by independent motors, rotating with different angular velocities. It was found that asymmetric rolling leads to microstructure modification and refinement. At low deformations one observes a process of grain size decrease caused by the asymmetry of rolling process. In contrast, at the medium range of deformations the microstructure refinement consists mainly in subgrain formation and grain fragmentation. Another observation is that for low to intermediate rolling reductions (≤40%) the predominant mechanisms are slip and twinning, while for higher deformation (>40%) the main mechanism is slip. It was found that grain refinement effect, caused by the rolling asymmetry, persists also after recrystallization annealing. And finally, texture homogenization and reduction of residual stress were confirmed for asymmetrically rolled samples.

Keywords: metals, asymmetric rolling, electron backscattering diffraction (EBSD), twinning, texture

1. INTRODUCTION

Titanium exhibits good corrosion resistance, low density and relatively high, although often insufficient, strength, which is why alloyed titanium is commonly used. Unfortunately, some alloying elements used for titanium strengthening appear to be toxic (e.g., the vanadium used in the standard alloy Ti-6Al-4V for its outstanding strength). Moreover, the biocompatibility of pure titanium is the highest among the main metallic biomaterials. All long-term effects of the reactions of the alloying elements on the human body are not well known, so the safest way is to use pure titanium traditionally strengthened by oxygen. The oxygen content in commercially pure titanium increases with the titanium grade number, causing an increase in yield strength at the expense of ductility and formability. However, oxygen significantly increases the susceptibility for stress corrosion cracking, therefore titanium grades 3 and 4 (with oxygen levels above the threshold of 0.20%) are typically avoided by users when chloride media are to be encountered (e.g., sea water or saline). The optimal combination of strength and susceptibility for stress corrosion cracking is thus obtained with titanium grade 2. This material is also valuable in many no-biomedical applications like aeronautic applications, chemical processes and marine equipment. Further strengthening of titanium without modification of its chemical composition is possible by plastic deformation.

Cold deformation is indeed a way of forming that can ensure increased strength, a required shape and size and good surface quality. For example, 40% of cold deformation almost doubles the tensile strength while the elongation at fracture falls to one third (ca., 6%) compared to the non-deformed material. In order to prevent internal damage, cold forming is usually followed by a heat treatment. The final annealing is applied in order to adjust the strength and elongation, to improve the resistance to cracking of the final product and to control the grain size. Grain refinement is classically promoted by high rolling reductions but, in conventional rolling practice, maximal reduction is limited by the resistance of the mill construction. In order to achieve the desired properties of the product, some optimized recrystallization and

*Corresponding author: wierzbanowski@fis.agh.edu.pl

cold rolling procedures were elaborated for traditional rolling process, i.e., for symmetric rolling.

However, rolling forces can be significantly reduced if asymmetrical rolling is applied. In such a rolling mode (also called asynchronous rolling), the peripheral velocities of the top and bottom rolls are different [1-5]. The velocity difference can result from dissimilar angular velocities or diameters of the rolls, or different friction coefficients between the two rolls and the processed material. Asymmetrical rolling can also cause a pronounced modification of the material properties and microstructure. A strong additional shear stress, which is induced during this type of deformation, can lead to enhanced grain fragmentation and texture homogenization throughout material thickness and reduction of residual stresses. Moreover, it influences the rolled plate shape (which can have a beneficial or detrimental effect) [6]. The degree of rolling asymmetry is usually limited as high asymmetries can be a reason for unacceptable vibrations of the stand and/or the slippage between the rolls and material. Previously published works on asymmetric rolling are mainly devoted to cubic structure metals [1-4,6,7]. In the case of h.c.p. metals there are many articles concerning asymmetrically rolled magnesium (e.g., [8,9]), but less numerous are the works devoted to titanium (e.g., [10]). Therefore, in the present work, a study of the microstructure of titanium grade 2 rolled asymmetrically and also annealed is presented.

2. EXPERIMENTAL PROCEDURE

Samples (of a size of 60x30x8 mm^3) of a commercially pure titanium grade 2 were symmetrically and asymmetrically rolled on a laboratory mill conceived by Simões *et al.* [7] and installed in the LSPM Laboratory (University Paris 13). The diameter of the rolls is equal to 180 mm. The rotation rate of the bottom roll (ω_2) was kept constant at 10 rpm (revolutions per minute) whereas that of the top roll (ω_1) was set equal to 10, 13, 15 rpm successively, so that the rolling asymmetry ratio ($A=\omega_1/\omega_2$) was set equal to 1.0, 1.3 and 1.5. In order to increase the friction between the rolls and the material, lubrication was not applied and the rolls' surfaces were ground by silicon carbide paper no. 80. Applied rolling reductions and number of passes for the examined specimens are listed in Table 1. The selected rolling schedules (i.e., rotation rates and partial reductions) ensured the deformed material was free of rolling defects such as cracks or end slivers. Before rolling, the upper and lower surfaces of the sample were identified; unidirectional rolling was then applied and the samples were not rotated between passes. For the weakly deformed specimens (i.e., up to a rolling reduction of 20% and 40%), the main microstructure characteristics of the deformed state could be determined and analyzed with the electron backscattering diffraction (EBSD) technique (see below). For the highly deformed samples (rolling reductions of 60%, 70%, and 80%), the microstructure characteristics were determined after annealing performed during 1 hour at 550 °C. The actual duration and temperature of the annealing treatment were chosen based on hardness tests in order to study the material right at the end of the primary recrystallization.

Table 1. Number of passes selected for each imposed rolling reduction

Rolling reduction	Number of passes
20%	4
40%	8
60%	11
70%	13
80%	15

The microstructure and crystallographic texture were characterized by EBSD measurements performed on the longitudinal cross-section, parallel to the ND-RD plane (where ND is the direction normal to the rolling plane and RD is the rolling direction). The observation area was always taken in the center of the rolled piece width. A scanning electron microscope (SEM) Zeiss Supra 40VP was used for the low deformed materials and some orientation images (OIs), of a size 350×300 μm^2, were determined with a step size of 0.3 μm. The highly deformed and, next, annealed materials were investigated with a Cambridge S360 (W-GUN) scanning electron microscope and OIs, of a size of 400×200 μm^2, and determined with a step size of 0.5 μm in this case. The filtering procedure of measurement data excluded grains containing less than 5 measurement points. The results of the EBSD measurements were analyzed with OIM TSL© v. 6.1 software. The presented EBSD maps show the topology of the orientation distributions of ND in the crystal reference frame (i.e., the 001 inverse pole figures). The microstructure was then quantified by: a) average grain area (μm^2), b) Kernel average misorientation, and c) average grain orientation spread [11]. The orientation distribution functions (ODFs) of the crystallographic textures were also calculated from the EBSD maps, assuming the hexagonal crystal symmetry and triclinic sample symmetry, using Bunge notation of the Euler angles [12]. As ODF sections $\varphi_1=0$ are sufficient for texture characterization of the investigated material, only these sections are shown. The presented misorientation angle distributions (see further text) were calculated taking into account misorientations between neighboring measurement points (pixels). Before SEM examination, the samples were mechanically polished with silicon carbide paper down to grade 4000 and then electro-polished using Struers electrolyte A3.

The classical $\sin^2\psi$ diffraction method [13-14] was applied for the residual stress measurements. The Williamson-Hall method [15] was used for the analysis of the diffracted line profile. X-ray patterns were recorded using a PANalytical

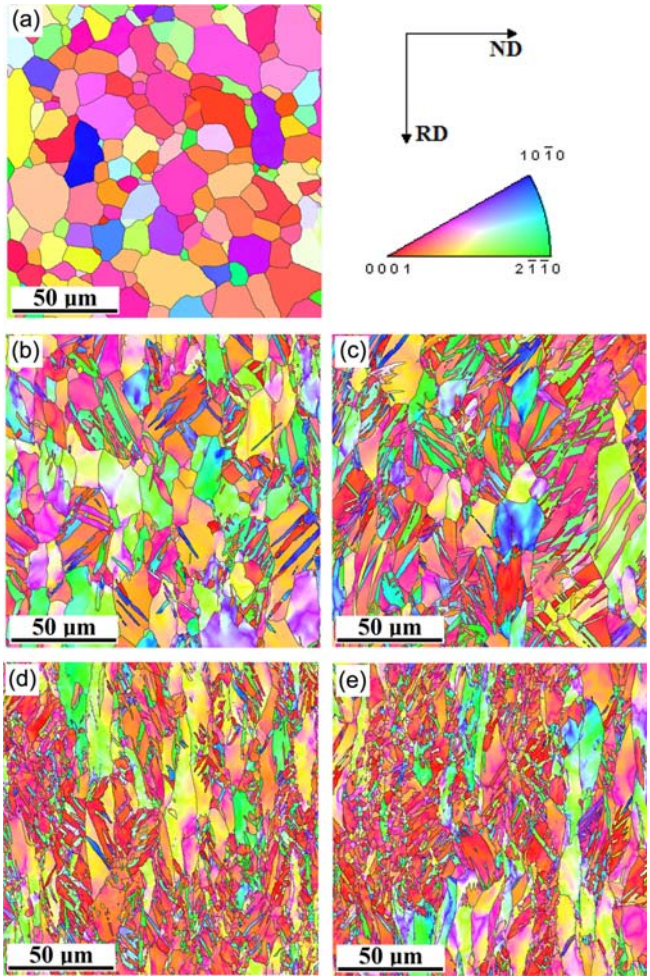

Fig. 1. Orientation images of size 150×150 µm^2 for the initial material (a), for the samples rolled symmetrically (A=1) and asymmetrically (A=1.3 and A=1.5) to the reductions of 20% (b, c) and 40% (d,e). EBSD measurements were performed on the longitudinal cross-section (ND-RD plane).

Empyrean diffractometer (CuKα radiation, wavelength λ= 1.54056 C) equipped with a parallel beam X-ray Göbel mirror and Soller slits in the incidence beam optics and parallel plate collimator, Soller slits and Ni β-filter in the front of Medipix2 detector PIXcel^{3D}. The X-ray measurement was performed on the rolling plane after removing (by etching and electropolishing) a 30 µm thick layer from both rolled surfaces (top and bottom).

3. RESULTS AND DISCUSSION

3.1. Microstructure of rolled titanium

Typical OIs for the central layers of the initial material and of the deformed samples are shown in Fig. 1. The presented microstructure of the initial material is very similar to that published in [16] for the same material. As can be seen in Fig. 1, the grain size quickly decreases with deformation, independently of the rolling asymmetry (i.e., value of A), and presumably mainly because of the occurrence of deformation twinning visible in all maps. The effect of symmetrical rolling on the average grain size calculated from the EBSD maps is shown in Fig. 2a. A distinct grain refinement is observed with increasing deformation. Moreover, it was also found that the average grain size of the material asymmetrically rolled up to 20% decreases with increasing rolling asymmetry A (Fig. 2b). For the rolling reduction of around 40%, we observe an increasing proportion of large and elongated grains along RD (Fig. 1d,e) but the influence of rolling asymmetry (A) on the grain size is not pronounced in this case (Fig. 2b). This effect is explained later in the text.

Two other factors characterizing the fragmentation of the microstructure, namely the *Kernel average misorientation* and the *average grain orientation spread*, are presented for samples rolled to the final reductions of 20% and 40% in Fig. 3. These parameters increase vs. with rolling reduction. They also increase vs. the degree of rolling asymmetry (both

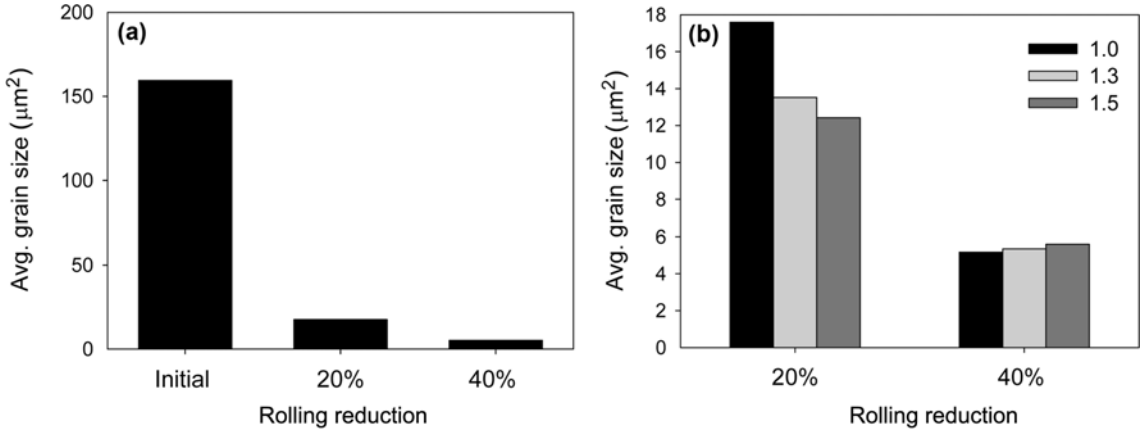

Fig. 2. Effects of rolling and of its asymmetry on the average grain area: (a) initial material and material rolled symmetrically (A=1) to 20% and 40% reductions, (b) material rolled to 20% and 40% reduction with three degrees of asymmetry: A=1, 1.1 and 1.5. Results for the center layers are shown.

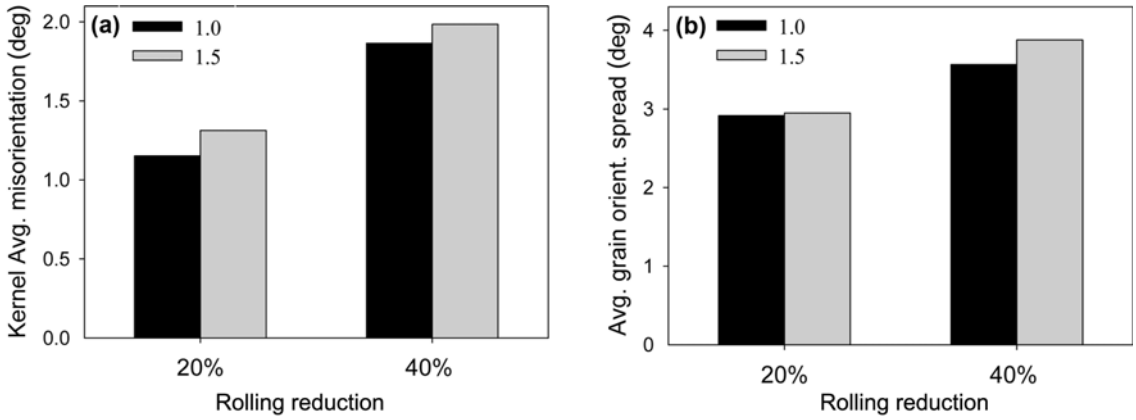

Fig. 3. Influence of rolling reduction (20% and 40%) and rolling asymmetry (A equal to 1.0 and 1.5) on: (a) Kernel average misorientation and (b) average grain orientation spread. The results for center layers are shown.

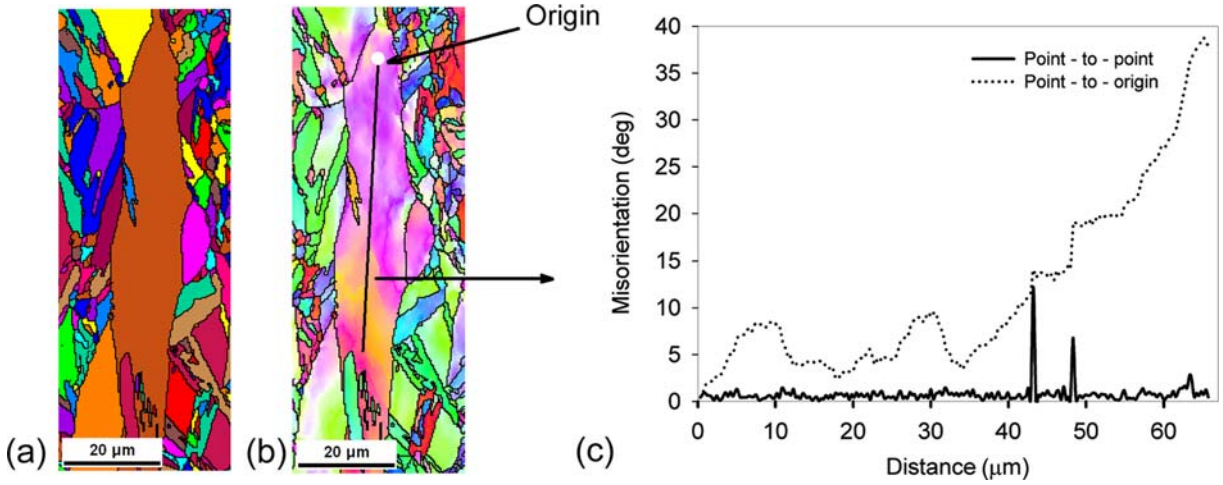

Fig. 4. EBSD maps presenting an elongated grain with high value of grain orientation spread in the sample rolled asymmetrically (A=1.5) to the reduction of 40%: (a) map showing grains defined on the basis of 15° misorientation, (b) orientation distribution map, and (c) misorientation profile along the line marked inside the grain.

for 20% and 40% reduction), which confirms the effect of more intense grain fragmentation during asymmetric rolling than during symmetric one.

As stated above, for the samples deformed up to 40% we do not observe a decrease of an average grain area vs. rolling asymmetry A (contrary to the case of lower deformations) but another grain refinement process appears at this strain. It consists in the continuous increase of the *intragranular* local spread in large grains, which are surrounded by strongly deformed and twinned material. An example of such a grain, for A=1.5, is shown in Fig. 4a,b. In OIM TSL software a grain is defined as a set of points with misorientation angles between neighboring measurement pixels smaller than some threshold value (15° in the present case). According to this approach, the point-to-point misorientation in a grain is generally quite small but the orientation difference between distant points in a grain can be relatively large. As an example, the misorientation profile in the studied big grain along the line marked in Fig. 4b is shown in Fig. 4c. The misorientation between the origin of the line (marked in Fig. 4b as a white circle) and a given point increases with distance and goes up to 40° in the studied case. It is evidently different than misorientations calculated point-to-point, which are generally very low. However, two low angle grain boundaries are formed in the presented grain, which are visible in the point-to-point misorientation distribution as two peaks in Fig. 4c. These subgrains potentially will become new grains and will thus contribute to the grain refinement with increasing strain.

Based on these results, one can conclude that asymmetric rolling produces quite fragmented microstructure inside grains of unalloyed titanium. This example explains our previous result: at 40% reduction the average size of grains does not decrease vs. the rolling asymmetry (Fig. 2b) but the internal fragmentation of grains increases, which is expressed by the increase of the average grain orientation spread and the

Kernel average misorientation (Fig. 3).

The mechanism of increasing the average grain orientation spread inside grains was discussed above and is explained in Fig. 4. This mechanism does not involve the decrease of the average grain size at medium deformations (around 40% rolling reduction). It is evident, however, that grain refinement vs. rolling asymmetry occurs at higher deformations, which has been shown using TEM observations (see, e.g., [10,17]. In the present work the study of grain refinement at higher deformations was performed for the rolled and annealed samples using the EBSD technique. The applied annealing assured the recovery of internal grain substructure and, in consequence, a reliable analysis of the EBSD maps was possible. In fact the influence of rolling asymmetry on grain refinement at higher strains (in the range of 60%-80%) was confirmed; these results are presented in Section 3.4.

It should be noted that the grain refinement observed in the initial range of deformation is mainly due to a strong twinning activity, and it is interesting to explain why a series of twins comes ahead of slip. A very probable explanation of this effect is that, in the initial sample (with initial characteristic texture), the slip systems are unfavorably oriented with respect to the applied rolling forces; this involves the activation of twinning systems, which are better oriented, and they are very active till around 20-30% strain. Next, after this stage of deformation, the twinned (i.e., reoriented) grains have much more favorable orientations for slip. Also other grains changed their orientation during the first stage of deformation. Hence, a further deformation proceeds, mainly by slip.

3.2. Twins in rolled titanium

As stated above, the refinement of titanium microstructure during rolling is mainly related to the mechanical twinning, which is an important mechanism of plastic deformation in titanium and in other h.c.p. metals. Therefore the proportions of twins present in the studied microstructures were also investigated. Three main types of deformation twins are reported to be active in titanium alloys, each of them being associated with a characteristic misorientation. These are the compressive twins (CT) associated with a 64.6° <10$\bar{1}$0> misorientation, the tensile twins type 1 (TT1) with 84.8° <11$\bar{2}$0> misorientation and type 2 (TT2) with 35.1° <10$\bar{1}$0> misorientation. Moreover, multiple twin configurations of twins appearing inside already twinned parts can also be formed. They also produce particular misorientations such as, for example, double twin, DT (i.e., TT1 twin formation inside a CT one) with resulting 41.2°<41$\bar{5}$3> misorientation with matrix [18]. The presence of twins can be revealed by the analysis of the misorientations between neighboring pixels in OIs. The misorientation distribution for the initial and symmetrically rolled materials is shown in Fig. 5 (to avoid the influence of the dislocation substructures, only misorientations higher than 15° were considered).

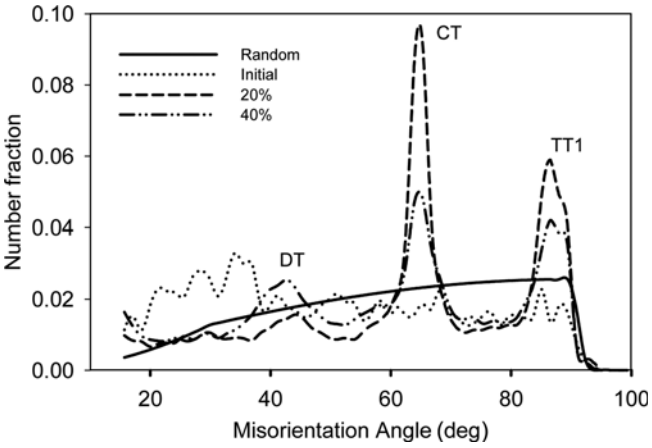

Fig. 5. Distribution of misorientation angle for titanium samples: random sample, initial material and the material rolled symmetrically (A=1) to the reductions 20% and 40%.

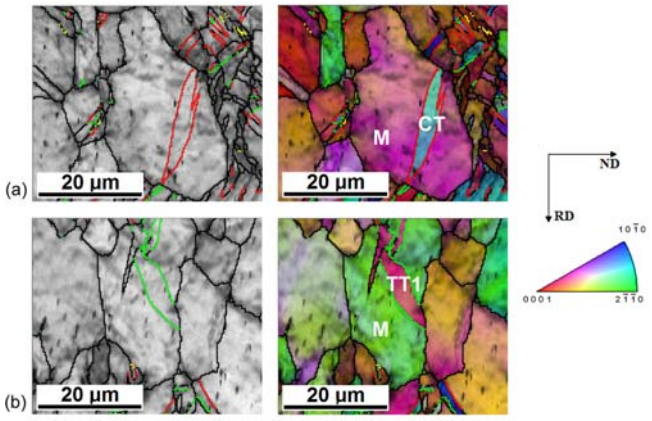

Fig. 6. EBSD map for the material rolled symmetrically to 20% reduction, displaying the occurrence of twins: (a) CT, (b) TT1. In the left column the boundaries with twin misorientations highlighted on the gray scale OIs are shown. In the right column the colour orientation maps are shown, where two particular matrices (M) and twins (CT) and (TT1) are marked. The following colours were used for boundaries: red: 65° <10$\bar{1}$0> misorientation (includes CT); green: 85° <11$\bar{2}$0> misorientation (includes TT1); yellow: 41° <41$\bar{5}$3> misorientation; black: other boundaries with misorientation higher than 15°.

The peak related to the tensile twin type 2 (TT2) is not observed in the presented misorientation distribution, and therefore this type of twin was not taken into account in what follows. In the initial material the twin related misorientations are rather absent in the misorientation distribution plot (Fig. 5) and consequently the amount of twins is very small. It is worth noting that the misorientation profile for the initial material contains some wide peaks below 40°, similar to the ones previously observed in rolled and annealed Zr [19], which were attributed to the presence of orientation fibers composing the initial texture.

A twin boundaries were found in the EBSD maps based on the identification of characteristic rotations axis and angles.

Table 2. Fractions of the total grain boundary length (with misorientations larger than 15°) for selected characteristic misorientations, defined with 5° tolerance for misorientation angle and for misorientation axis, after symmetrical rolling (A=1.0) up to 20 and 40% reduction

	Rolling reduction	
	20%	40%
65° <10$\bar{1}$0> (CT)	22.2%	11.2%
85° <11$\bar{2}$0> (TT1)	14.9%	9.2%
41° <41$\bar{5}$3> (DT)	0.9%	2.9%

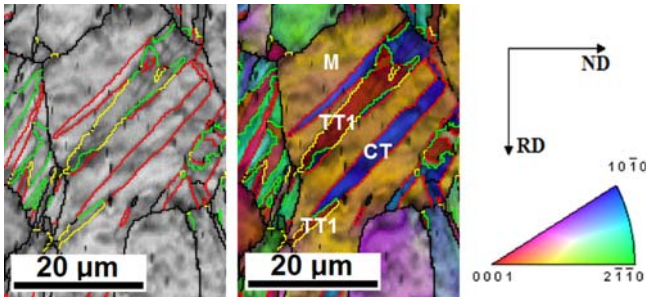

Fig. 7. Example of the formation of TT1 twin inside a CT one in the material symmetrically rolled to 20% reduction. The following colours were used for boundaries: red: 65°<10$\bar{1}$0> misorientation (includes CT); green: 85° <11$\bar{2}$0> misorientation (includes TT1); yellow: 41° <41$\bar{5}$3> misorientation; black: other boundaries with misorientation higher than 15°.

This identification has to be done with some tolerance. In most works the angular tolerance of 5° is used (e.g., in [18,20]. After performing some additional tests we have also used this value. The OI map, revealing the occurrence of CT and TT1 twin in 20% rolled titanium is shown in Fig. 6, while the corresponding percentages of various twin boundaries are listed in Table 2.

Both types of twins appear significantly at 20% rolling reduction. The percentage of CT is almost two times higher than that of TT1 (Fig. 5, Table 2). On the other hand the proportion of the 41° <41$\bar{5}$3> misorientation (DT double twins) is already higher than the random value. A detailed analysis of the OIs confirms that this misorientation results from the TT1 formation inside CT twins [21,22] (as shown in Fig. 7). It is worth noting that it was also found that in an unalloyed titanium rolled to 10% reduction at 720 °C, one observes a much larger amount of TT1 twins than CT ones and only a slightly increased amount of DT misorientation [23]. As such, one can conclude that the rolling temperature significantly modifies the relative proportions of different twinning families.

The present results show that increasing the rolling reduction from 20% to 40% significantly reduces the amount of TT1 and CT misorientations, and especially the CT twins disappear much faster than the TT1 ones (cf., Table 2) - a similar effect of decreasing the twinned volume fraction vs. deformation was reported in [24]. This decrease of the simple twin misorientations is accompanied by a simultaneous small increase of the amount of the double twin (DT) misorientation. Next, above a 40% rolling reduction, a significant part of the material is already strongly reoriented by twinning and further deformation proceeds mainly by slip.

The influence of the rolling asymmetry on twinning is summarized in Table 3. One can see that at 20% rolling reduction there is a moderate tendency of increasing the twin volume with rolling asymmetry: the fractions of TT1 and DT twins increases when passing from A=1 to A=1.5 and the fraction of CT twins increases when passing from A=1 to A=1.3. It should be added that at low and intermediate rolling reductions (< 40%) the twinning mechanism plays an important role, besides the slip. In contrast, in the case of 40% (and higher) rolling reduction a general tendency is a decrease of twinning activity (cf., Table 2) and the main deformation mechanism becomes slip. The increase of rolling asymmetry from 1 to 1.5 at this rolling reduction induces a further systematic decrease of the fractions of three types of twins (Table 3).

3.3. Textures and residual stress

The effects of asymmetric rolling - relatively difficult to analyze at the local grain scale - can also be studied through more global parameters such as crystallographic texture and internal and residual stresses (e.g., [26-29]). The textures of the initial material and of the material rolled to 40% reduction are shown in Fig. 8. The representative $\varphi_1=0^0$ sections (cf., [12]) of the orientation distribution function (*ODF*) are shown in this Figure. One can observe that the main texture

Table 3. Influence of rolling asymmetry, A, for titanium samples rolled to 20% and 40% on the fractions of the three characteristic twin misorientations (defined with 5° tolerance for misorientation angle and axis). The boundaries with misorientations higher than 15° were taken into account

	Rolling reduction					
	20%			40%		
$A=\omega_1/\omega_2$	1.0	1.3	1.5	1.0	1.3	1.5
65° <10$\bar{1}$0> (CT)	22.2%	23.2%	20.1%	11.2%	9.1%	8.4%
85° <11$\bar{2}$0> (TT1)	14.9%	13.6%	18.1%	9.2%	7.3%	7.8%
41° <41$\bar{5}$3> (DT)	0.9%	0.9%	1.3%	2.9%	2.6%	2.1%

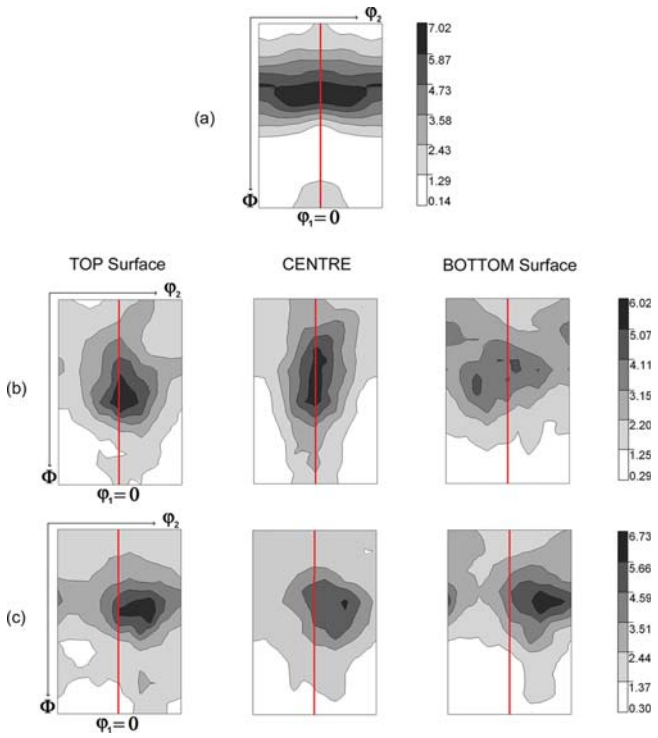

Fig. 8. Textures of titanium (grade 2) determined by EBSD technique: homogeneous texture of initial material (a), textures in three material layers (top, center, bottom) after symmetric rolling (b), and after asymmetric rolling (A=1.3) (c); rolling reduction is 40%.

maxima of the initial material and the material rolled symmetrically and measured in the central layer are located in symmetrical positions with respect to the red line plotted at $\varphi_2=30^0$ (Fig. 8a,b). Only in the layers close to the top and bottom surface of the symmetrically rolled specimen, some asymmetry in the positions of the maxima can be observed (i.e., shifts to the right and to the left, respectively) - Fig. 8b. In contrast, in the case of the asymmetrically rolled material, a significant shift of texture maxima to the right is observed over the whole thickness of the rolled bar (Fig. 8c). The discussed shifts of maxima correspond to texture rotations around the transverse direction (TD) of the rolled bar. The results presented in Fig. 8 show that the texture of the asymmetrically rolled material is more homogeneous than that of the symmetrically rolled one. The above results were confirmed by the modeling of texture development using the Finite Element Method [29] with an implemented crystalline model for plastic deformation, as described elsewhere [30,31]. It was shown that rotations of texture, also observed in the present work, are caused by a characteristic distribution of the internal shear stress component $\sigma_{RD\text{-}ND}$ across the thickness of the rolled bar [29]. It was found that during asymmetric rolling a nearly homogeneous distribution of this stress component can be obtained, which leads to a homogeneous texture.

Table 4. Residual stress components [MPa] measured in the top and bottom surface layers of symmetrically and asymmetrically rolled titanium samples (A=1 and A=1.5); rolling reduction 80%

	Top surface		Bottom surface	
	$\sigma_{RD\text{-}RD}$	$\sigma_{TD\text{-}TD}$	$\sigma_{RD\text{-}RD}$	$\sigma_{TD\text{-}TD}$
$A=\omega_1/\omega_2=1$	-87.8 ± 18	-128.6 ± 18	-108.6 ± 18	-65.9 ± 18
$A=\omega_1/\omega_2=1.5$	-60.4 ± 14	-104.2 ± 14	-37.7 ± 18	- 37.4 ± 18

Table 5. Average size of coherent domain, (d) and the average lattice distortion (e) in the top and bottom surfaces of titanium rolled symmetrically and asymmetrically to the reduction of 80%. The relative error of the measured quantities is ca. 10%

	Top surface		Bottom surface	
	d Å	ε %	d Å	ε %
$A=\omega_1/\omega_2=1$	1890	0.40	2590	0.41
$A=\omega_1/\omega_2=1.5$	1160	0.38	640	0.34

As residual stresses play an important role in mechanical and thermodynamic properties of materials (e.g., [32,33]) they were measured for the studied materials using X-ray diffraction. In addition, analysis of the diffraction peak shape was also carried out. The most significant results of residual stress analysis were found for the samples deformed up to 80% strain, and in consequence these results are presented below. The stress measurement results are shown in Table 4. The two non-zero residual stress components detected on the top and bottom sample surfaces (i.e., $\sigma_{RD\text{-}RD}$ and $\sigma_{TD\text{-}TD}$) are compressive in all the presented cases. The magnitudes of residual stress components are significantly lower in the asymmetrically rolled samples (A=1.5). This tendency is especially visible in the bottom surface layer of the material. This effect is probably due to the fact that deformation is more homogeneous through the thickness of the specimen after asymmetric rolling (more homogeneous deformation reduces residual stresses).

The average size of coherent domain (*d*) and the average elastic lattice distortion (*e*), determined for both surfaces of the symmetrically and asymmetrically rolled titanium samples using the Williamson-Hall method [15], are presented in Table 5. For each of two investigated sample surfaces we observed a reduction of *d* and ε when passing from symmetrical (A=1) to asymmetrical (A=1.5) rolling mode, though this effect appears much stronger on the bottom surface, as for residual stress (cf., Tables 4 and 5).

3.4. Microstructure and texture of the annealed material

As was expected, a higher degree of deformation also leads to a decrease of the grain size of the annealed material for each rolling mode tested in the present research. This is quite clear from Fig. 9 which shows *OI*s from the central layers of the materials rolled symmetrically to 60%, 70% and 80% reductions. This result is confirmed in Fig. 10a, where a bar

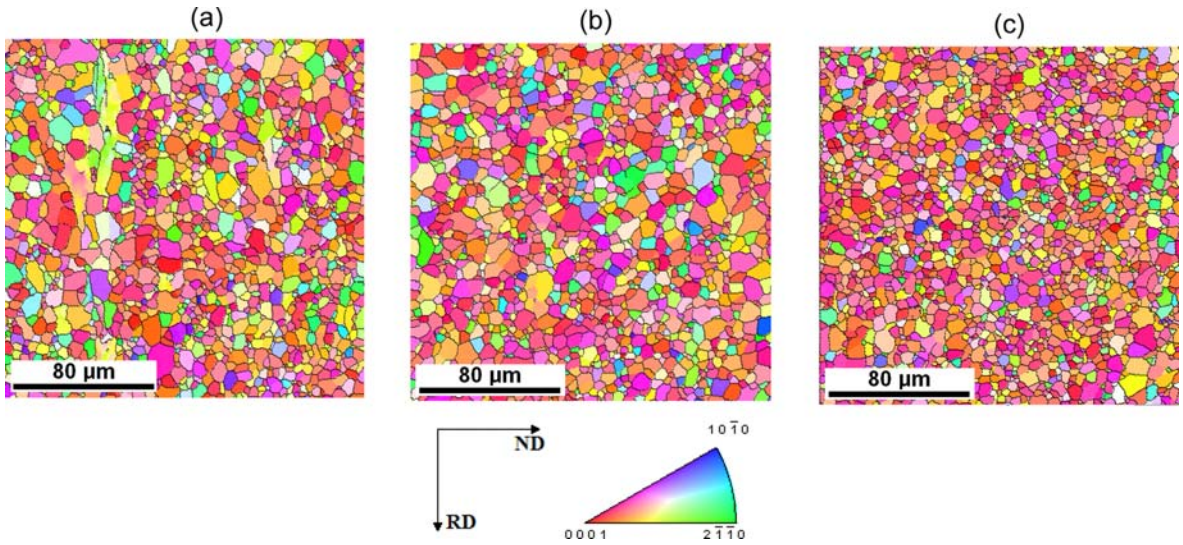

Fig. 9. Orientation maps of 200×200 μm^2 size for centre layers of titanium annealed during 1 h at 550 °C after symmetric rolling (A=1) to the reductions of: 60% (a), 70% (b), and 80% (c). EBSD measurements were performed on the longitudinal cross-section (ND-RD plane).

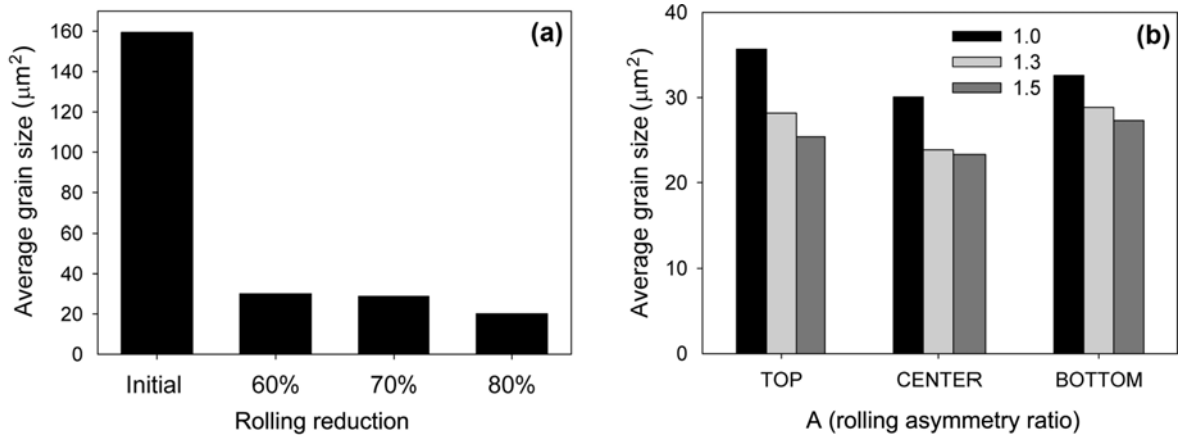

Fig. 10. Average grain size (μm^2) of: (a) the initial material and of the samples rolled symmetrically (A=1) to 60%, 70%, 80% reductions and annealed during 1 h at 550° (results for centre layers are shown), (b) the samples rolled asymmetrically (A=1, 1.3 and 1.5) to 60% reduction and annealed during 1 h at 550 °C (results for top, center and bottom layers are shown).

chart showing the average grain areas of the initial material and of the samples annealed after rolling is presented. Additionally, rolling asymmetry further enhances the refinement on the rolled and annealed material. This is especially visible in the case of titanium rolled to 60% reduction and further annealed (Fig. 10b), where asymmetric rolling leads to smaller average grain size than the symmetric process (A=1). In this figure, the average grain area is shown for three layers of the sample (top, center, bottom) and for three degrees of rolling asymmetry (A=1.0, A=1.3 and A=1.5). We observe a grain refinement after asymmetric rolling in the three examined layers. In the samples rolled to 70% and 80% reductions, the grain refinement in the annealed samples starts when passing from the rolling asymmetry A=1.3 to A=1.5.

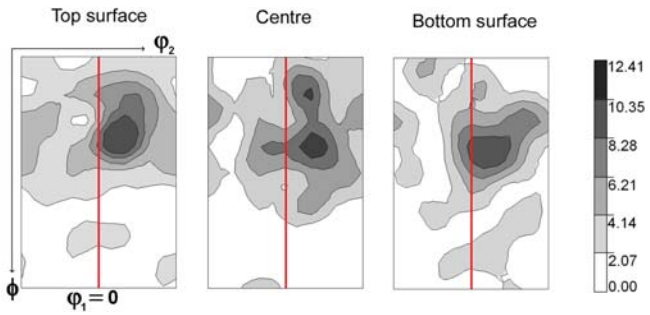

Fig. 11. Textures after asymmetric rolling (A=1.3, 40% reduction) and annealing during 1 h at 550 °C. The φ_1=0 sections are shown and red lines are located at φ_2=30°, as in Fig. 8.

The texture after asymmetric rolling and annealing is shown in Fig. 11. It can be seen that the characteristic shift to the right of the texture maxima appearing in the three sample layers after asymmetric rolling (cf., Fig. 8c) persists after annealing. Hence, in this sense the texture stays homogeneous also after annealing. It should be added that the misorientation angle distributions for the samples after symmetric and asymmetric rolling, followed by annealing, were also examined. These distributions were practically the same and, moreover, similar to that of the initial material shown in Fig. 2. Therefore, the misorientation characteristics of the rolled and annealed material do not depend on the rolling asymmetry.

Finally, one can conclude that asymmetric rolling favors grain refinement. Moreover, the texture homogenization induced by asymmetric rolling persists after recrystallization.

4. CONCLUSIONS

The presented results show that asymmetric rolling of the polycrystalline titanium (grade 2) leads to the following modifications of material properties (as compared to symmetric rolling):

Generally finer grains are obtained from the samples rolled asymmetrically to 20% reduction;

The effect of grain refinement caused by asymmetric rolling also appears in highly deformed and annealed samples; it was found that the average grain size is distinctly smaller in the three material layers (top, bottom, center) of titanium rolled asymmetrically to 60% reduction and then annealed;

The intra-granular microstructure is more fragmented, which is expressed by an increase in the average grain orientation spread;

A nearly homogeneous texture across the sample thickness is formed after rolling, and this effect persists after annealing; the texture of asymmetrically rolled material is rotated around transverse direction as compared with that of the central layer of a symmetrically rolled material;

Residual stresses, coherent domain size and average lattice distortion in the surface layers of the asymmetrically rolled samples are distinctly reduced; this effect is more strongly marked in the bottom sample layer (corresponding to a slower roll). This effect can have potential applications in modifications of surface layers' properties;

Mechanical twinning plays an important role in the microstructure refining. At higher rolling reductions, the increase of the rolling asymmetry causes a decrease of twin fractions. This result is analogous to a general effect of a decrease of twin amounts with increasing deformation.

In summary, it can be concluded that asymmetric rolling should be applied for polycrystalline titanium when a finer microstructure, a more homogeneous texture and lower residual stresses are required.

ACKNOWLEDGEMENTS

This study was financed by the grants of Polish National Centre for Science (NCN) under decision numbers: DEC-2011/01/B/ST8/07394 and DEC-2011/01/D/ST8/07399.

REFERENCES

1. H. Gao and G. Chen, *Iron and Steel*, **33**, 63 (1998).
2. S. H. Lee and G. N, Lee, *Int. J. Mech. Sci.* **43**, 1997 (2001).
3. S. Chhann, D. Solas, A. L. Etter, R. Penelle, and T. Baudin, *Mater. Sci. Forum* **550**, 551(2007).
4. S. Wronski, B. Ghilianu, T. Chauveau, and B. Bacroix, *Mater. Charact.* **62**, 22 (2011).
5. F. Zhang, G. Vincent, Y. H. Sha, L. Zuo, J. J. Fundenberger, and C. Esling, *Scripta Mater.* **50**, 1011 (2004).
6. S. Wronski, K. Wierzbanowski, B. Bacroix, T. Chauveau, and M. Wróbel, *J. Cent. South Univ. T.* **20**, 1443 (2013).
7. F. J. Simões, R. J. Alves de Sousa, J. A. Grácio, F. Barlat, and J. W. Yoon, *Int. J. Mech. Sci.* **50**, 1372 (2008).
8. J.-H. Cho, S. S. Jeong, H.-W. Kim, and S.-B. Kang, *Mat. Sci. Eng. A* **566**, 40 (2013).
9. X. Huang, K. Suzuki, A. Watazu, I. Shigematsu, and N. Saito, *Mat. Sci. Eng. A* **488**, 214 (2008).
10. Z. Li, L. Fu, B. Fu, and A. Shan, *Mat. Sci. Eng. A*, **558**, 309 (2012).
11. Orientation Imaging Microscopy™ (OIM) Analysis 5.3 Software User Manual, EDAX/TSL, Utah, USA (2008).
12. H. Bunge, *Texture Analysis in Material Science*, pp.3-41, Butterworths, London (1982).
13. I. C. Noyan and J. B. Cohen, *Residual Stress: Measurement by Diffraction and Interpretation*, pp.17-163, Springer Verlag, New York (1987).
14. U. Wenzel, J. Ligot, P. Lamparter, A. C. Vermeulen, and E. J. Mittemeijer, *J. Appl. Crystallogr.* **38**, 1 (2005).
15. G. K. Williamson and W. H. Hall, *Acta Metall.* **1**, 22 (1953).
16. K. Ahn, H. Huh, and J. Yoon, *Met. Mater. Int.* **19**, 749 (2013).
17. Z. Li, L. Fu, B. Fu, and A. Shan, *Mater. Sci. Eng. A* **558**, 309 (2012).
18. N. Bozzolo, L. Chan, and A. R. Rollet, *J. Appl. Crystallogr.* **43**, 596 (2010).
19. B. Bacroix, J. Tarasiuk, K. Wierzbanowski, and K. Zhu, *J. Appl. Crystallogr.* **43**, 134 (2010).
20. S. Pamda, S. K. Sahoo, A. Dash, M. Bagwan, G. Kumar, S. C. Mishra, and S. Suwas, *Mater. Charact.* **98**, 93 (2014).
21. Y. B. Chun, S. H. Yu, S. L. Semiatin, and S. K. Hwang, *Mat. Sci. Eng. A* **398**, 209 (2005).
22. S. V. Zherebstov, G. D. Dyakonov, A. A. Salem, S. P. Malysheva, G. A. Salishchev, and S. L. Semiatin, *Mat. Sci. Eng. A* **528**, 3474 (2011).
23. T. Ungar, M.G. Glavicic, L. Balogh, K. Nyilas, A. A. Salem, G. Ribarik, and S.L. Semiatin, *Mat. Sci. Eng. A* **493**, 79 (2008).

24. Y. B. Chun, S. H. Yu, S. L. Semiatin, and S. K. Hwang, *Mat. Sci. Eng. A* **398**, 209 (2005).
25. S. Wroński, K. Wierzbanowski, B. Bacroix, M. Wróbel, E. Rauch, F. Montheillet, and M. Wroński, *Arch. Metall. Mater.* **54**, 89 (2009).
26. M. Wronski, K. Wierzbanowski, L. Pytlik, B. Bacroix, and P. Lipinski, *Mater. Sci. Forum*, **777**, 65 (2014).
27. S. Wroński, K. Wierzbanowski, B. Bacroix, M. Wróbel, T. Chauveau, and M. Wroński, *Mater. Sci. Forum*, **638-642**, 2811 (2010).
28. J. Tarasiuk, K. Wierzbanowski, and A. Baczmański, *Cryst. Res. Technol.* **33**, 101 (1998).
29. M. Wronski, K. Wierzbanowski, S. Wronski, B. Bacroix, and P. Lipinski, *Int. J. Mech. Sci.* **87**, 258 (2014).
30. K. Wierzbanowski, A. Baczmanski, P. Lipinski, and A. Lodini, *Arch. Metall. Mater.* **52**, 77 (2007).
31. A. Baczmański, K. Wierzbanowski, and J. Tarasiuk, *Z. Metallkd*. **86**, 507 (1995).
32. A. Baczmański, K. Wierzbanowski, J. Tarasiuk, M. Ceretti, and A. Lodini, *Rev. Metall-Paris*, **94**, 1467 (1997).
33. A. Baczmański, A. Tidu, P. Lipinski, M. Humbert, and K. Wierzbanowski, *Mater. Sci. Forum*, **524-525**, 235 (2006).